Tellus (1995), 47A, 502–524
Printed in Belgium – all rights reserved

TELLUS
ISSN 0280-6495

Flow over a mesoscale ridge: pathways to regime transition

By J. TRÜB and H. C. DAVIES*, *Institute for Atmospheric Physics, ETH, Zürich, Switzerland*

(Manuscript received 4 March 1994; in final form 29 August 1994)

ABSTRACT

A theoretical and modelling study is undertaken of an airstream of uniform flow (U) and stratification (N) impinging normally upon a two-dimensional bell-shaped ridge of half-width (L) and height (H) that is located on an f-plane. The associated Rossby number ($R_o = U/fL$) and inverse Froude Number ($F = NH/U$) are taken to be such that the effects of both the earth's rotation and non-linear processes can significantly influence the nature of the flow response. It is shown that within this intermediate meso-α/β scale sub-domain of (R_o, F) parameter space there are several distinctive signatures to the flow response, and each signature is associated with the generation of appreciable buoyancy wave energy. As R_o decreases across the sub-domain, the source for this wave energy changes continuously from the conventional direct orographic forcing of vertically propagating waves (for $R_o > 1$), to that linked with the cusping of a leeward train of low-level near-inertial waves (for $R_o \sim 1$), and thereafter to the forcing induced by the adjustment that accompanies the scale contraction of balanced flow (for $R_o < 1$). In effect this change highlights the various pathways to regime transition within the intermediate domain.

1. Introduction

Many elongated mesoscale mountain ranges in mid-latitudes, e.g., the European and Southern Alps, the Appalachians, the Pyrenees, and the Scandinavian Highlands, are characterized by a half-width $L \sim 50$–200 km and a mean ridge height $H \sim 500$–2000 m. Thus for an airstream incident normally upon such terrain the values of the Rossby number ($R_o = U/fL$) and inverse Froude Number ($F = NH/U$) lie characteristically in the range $R_o \sim [\frac{1}{2} - 2]$ and $F \sim [\frac{1}{2} - 2]$. At these intermediate values of (R_o, F), the effects of both the earth's rotation and non-linear processes can be significant. Moreover the width-to-length ratio ($\sim 1/10$) of these ranges suggest that the response can have a substantial quasi two-dimensional component.

It is the combined influence of rotation and nonlinearity in a quasi-steady, two-dimensional flow setting that forms the theme of the present theoretical study. To this end we consider an inviscid, Boussinesq and incompressible flow system, and base the study upon the paradigmatic configuration of an airstream of uniform flow and stratification impinging normally upon a two-dimensional ridge on an f-plane. In this setting R_o and F are the key dimensionless parameters, and a range of previous theoretical and numerical modelling studies have elicited the nature of the flow response in various sub-domains of the (R_o, F) parameter space.

In the limit of small ridge height ($F \ll 1$) linear theory provides an useful indication of the response (Gill, 1982). For $R_o > 10$, i.e., weak rotational influence- the hydrostatic response takes the form of almost non-dispersive buoyancy waves that propagate at a small angle to the vertical and exhibit an across ridge asymmetry with de/acceleration of the low-level flow up/downstream of the crest. For $R_o \sim 1$ the dominant perturbations take the form (Pierrehumbert, 1984) of inertia-buoyancy waves for $R_o \sim 1_+$ and pseudo-geostrophic waves for $R_o \sim 1_-$, and both are associated with comparatively large amplitude. The former are dispersive and characterized by

* Corresponding author's address: H. C. Davies, Institute for Atmospheric Physics, ETH, Hönggerberg HPP, 8093 Zürich, Switzerland.

very short vertical wavelength and quasi-horizontal energy propagation, whilst the latter are non-propagating and strongly evanescent. For $R_o \ll 1$ (i.e., strong rotational influence), the response for our meso-scale f-plane setting takes the form of quasi-geostrophic evanescent waves. (We note in passing that the inclusion of a β-effect would render a wave-like vertical structure to the ultra-long planetary waves.) The evanescent waves are symmetric relative to the crest and are associated with a mild decrease in the strength of the incident airstream and the static stability both up and downstream of the ridge, and a stronger speed-up and enhanced stability in the vicinity of the crest.

At higher values of F nonlinear processes will modify the forementioned responses, and in the limit of a very high ridge or strong stratification ($F \gg 1$) a transition to a radically different flow patterns is expected to prevail. In this context key sectors of the (R_o, F) parameter space are marked in Fig. 1. In the non-rotating limit, an increase in F enhances the amplitude of the buoyancy waves and results in a marked steepening of upslope portions of the undulations (Smith, 1977; Lilly and Klemp, 1979). At a value $F = F_I$, say, the upslope becomes vertical locally. Thus the criterion for convective overturning is attained and this marks a transition to a flow regime involving wave-breaking. A further increase to $F = F_{II}$ permits the amplitude of upstream propagating columnar modes to effect a complete retardation of the incident low-level flow, and this signals another regime transition to a pattern including upstream blocking (Pierrehumbert and Wyman, 1985; Baines, 1987). Rather less is known about the nature of the large amplitude response for non-infinite values of R_o. Theoretical studies (Pierrehumbert, 1985; Davies and Horn, 1988) reveal that an increase in F for $R_o \ll 1$ amplifies the evanescent features and that at $R_o F = (R_o F)_I$ the semi-geostrophic response breaks down. Also for intermediate values of R_o the numerical simulations of Pierrehumbert and Wyman (1985) indicate that as F increases a wave breaking regime precedes the transit to a partially blocked regime and this is demarked approximately by $R_o(F - F_{II}) = C$ (const.).

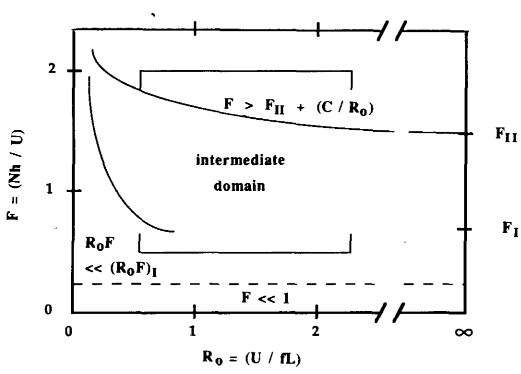

Fig. 1. Schematic depiction of the "intermediate domain" of the (R_o, F) parameter space. This domain is enclosed by the lines demarking small amplitude terrain ($F \ll 1$), the almost non-rotational limit ($R_o \gg 1$), the domain of semi-geostrophy $R_o F \ll (R_o F)_I$, and the criterion for blocked flow, $R_o(F - F_{II}) \sim C$.

The precise values of $\{F, (R_o F), \text{etc.}\}$ for the various criteria mentioned above depend upon the shape of the orography. Irrespective of their exact values we note that the character of the flow has been examined in the limit of small amplitude terrain ($F \ll 1$), the almost non-rotational limit ($R_o \gg 1$), and the domain of semi-geostrophy $R_o F \ll (R_o F)_I$. Together with the bound placed by the criterion for blocked flow, $R_o(F - F_{II}) \sim C$, these regions circumscribe and form the margin for the forementioned "intermediate domain" of the parameter space (see Fig. 1).

Here the objective is to examine the nature of the flow patterns and the pathway(s) to regime transition within this "intermediate domain". It is instructive to note that in this domain the large amplitude of the inertia-buoyancy waves and the strongly evanescent structure of the semi-geostrophic response are both indicative of the onset of nonlinear effects at small values of F. Yet neither of these features directly presage the regime transition associated with wave-overturning and/or upstream blocking. This conundrum is explored using a complementary mix of theoretical considerations and numerical model simulations. The former provides a framework for the numerical modelling strategy and a rudimentary base for understanding the resulting simulated flow patterns.

2. Preliminary theoretical considerations and a hierarchy of models

Theoretical considerations of small amplitude waves and of the semi-geostrophic flow system have yielded considerable insight to the nature of mesoscale orographic flow. However flow features that signal a regime transition, e.g., wave overturning and upstream blocking, are inherently nonlinear and their study is beyond the limit of linear wave theory. Likewise semi-geostrophic theory can not itself determine what prevails beyond its own breakdown. Nevertheless these approaches can at least provide a qualitative guide to the influence of rotation upon the finite-amplitude orographic flow response, and indicate where in parameter space and within what form of physical features, nonlinear and/or unbalanced effects will first attain importance.

In this section, we summarize, refine and extend aspects of existing theory that pertain to regime transition and do so using a hierarchy of idealized models.

2.1. *The Non-hydrostatic nonlinear flow system*

For our paradigmatic configuration of an incident flow of uniform velocity (U) and stratification (N) on an f-plane the equations governing nonlinear perturbations away from this basic state take the form,

$$L(u) - fv = -p_x, \tag{1a}$$

$$L(v) + fu = 0, \tag{1b}$$

$$L(w) = -p_z + b, \tag{1c}$$

$$u_x + w_z = 0, \tag{1d}$$

$$L(b) + wN^2 = 0, \tag{1e}$$

with L defining the material derivative such that

$$L(A) = A_t + (U+u)(A)_x + w(A)_z.$$

Here subscripts denote derivatives, small case letters signify perturbation variables, the symbol b (defined by $(g\theta/\Theta)$) denotes the perturbation parcel buoyancy, and p is the pressure perturbation scaled by the density. The remaining notation is standard.

In subsequent sub-sections, we consider several limit forms of this system but here we first consider features of this system itself. It possesses steady nonlinear wave solutions of the form,

$$(u, w, p) = (u^*, w^*, p^*)\cos(kx + nz + \varphi), \tag{2a}$$

$$(v, b) = (v^*, b^*)\sin(kx + nz + \varphi). \tag{2b}$$

These solutions exist provided the Rossby number (defined for the present in terms of the wavenumber k) is such that $R_o = (Uk/f) > 1$ and $S = (Uk/N) < 1$. They represent upstream sloping inertia-buoyancy waves and these formulae extend the available nonlinear solutions for the non-rotating limit to include rotational effects.

The full streamfunction, i.e., the basic state plus perturbation, in an (x, z) section of the three-dimensional streamline pattern is prescribed by,

$$\psi = -U[z - H\sin(kx + nz + \varphi)], \tag{3}$$

and the underlying terrain, $\eta(x)$, is defined (setting say, $\psi = 0$) by the transcendental equation,

$$\eta(x) = H\sin(kx + n\eta + \varphi). \tag{4}$$

The perturbations are such that the (k, n) wavenumber-pairing satisfy the relationship,

$$(n/k)^2 = (N/f)^2\,[1 - S^2]/[R_o^2 - 1],$$
$$\text{with}\quad S = (Uk/N) = (f/N)\,R_o, \tag{5}$$

and their polarization is such that,

$$(u^*/U) = (nH), \qquad (w^*/U) = -(kH),$$
$$(v^*/U) = (R_o)^{-1}\,(nH), \tag{6a}$$

$$(b^*) = -(N^2H), \tag{6b}$$

$$(p^*/U^2) = -\frac{\{(N/f)^2 - 1\}(nH)}{\{(R_o)^2\,[1 + (n/k)^2]\}}. \tag{6c}$$

Eqs. (5–6) indicate that as R_o decreases toward unity, the vertical wavenumber (n) and the velocity components (u, v) tend to infinity, whilst the pressure perturbation tends to zero. (Note that this singularity at the inertial scale prevails even for finite amplitude perturbations.) Also eq. (3) indicates that the rotation renders the nonlinear streamline displacement (and the profile of the underlying terrain) a non-sinusoidal periodic form with steeper narrower upslopes and flatter broadened downslopes. Furthermore, it can be shown that for these wave solutions:

the criterion for flow overturning, $(U + u) < 0$, is satisfied if $nH > 1$, i.e.,

$$F^2 > \{1 - (R_o)^{-2}\}/\{1 - S^2\}$$
$$\text{with}\quad F = (NH/U); \tag{7}$$

the minimum value for the Richardson Number, $R_i = N^2/|v_z|^2$, is

$$R_i = \frac{1}{2}\{1-S^2\}^{-1}\left[1-\left\{\frac{1-F^2(1-S^2)}{(1-R_o^{-2})^2}\right\}^{1/2}\right]^{-1}; \tag{8a}$$

the necessary condition for Kelvin–Helmholtz (K–H) instability of an uni-directional horizontal flow ($R_i < \frac{1}{4}$) is satisfied provided

$$F^2 > \{1-(R_o)^{-2}\}^2/\{1-S^2\}; \tag{8b}$$

the width of the steepened upslope contracts to a singularity as

$$nH \to (\pi/2) \qquad \text{from below,}$$

i.e.,

$$F^2 \to (\pi/2)^2\{1-(R_o)^{-2}\}^2/\{1-S^2\}. \tag{9}$$

The criteria expressed in eqs. (7–8) represent the f-plane extension of earlier formulae applicable to non-rotating systems (Lilly and Klemp, 1979).

It follows from these equations that, *for a single wave component* and in comparison with the non-rotational limit ($f = 0$), the influence of rotation reduces the orographic amplitude necessary to satisfy the criteria for both overturning and K–H instability. This is consistent with linking the higher amplitude of the (u, v) velocity perturbations of inertia-buoyancy waves with the likelihood of an earlier regime transition.

2.2. *The hydrostatic linear flow system*

Terrain with a meso α or β scale width generate predominantly hydrostatic inertia-buoyancy waves. Moreover relationships (eqs. (2–6)), shown earlier to be valid in the nonlinear limit, are also those that pertain for small amplitude inertia-buoyancy waves (Gill, 1982), and their hydrostatic limit-form are obtained by setting $S = 0$. (Recall that for meso-α or β scale terrain $R_o \sim 1$ or less and for typical atmospheric conditions $f/N \ll 1$, so that it follows from eq. (5) that $S \ll 1$).

Here the reduced hydrostatic form of eqs. (2–6) are adopted to examine the linear response to a localized meso α or β scale orographic feature. In particular we consider the role of rotation in modifying, via amplitude and dispersion effects, the conditions favourable for flow-overturning.

Using standard wave theory results we infer sequentially the spatial location(s) and amplitude of the perturbed downstream flow component at the location where conditions will be most conducive to wave-overturning. From eq. (5) it can be deduced that the (x, z)-directed group velocities (u_g, w_g) of a steady-state wave packet are given by (Gill, 1982, p. 264),

$$u_g = U[1 - N^2/(nU)^2],$$
$$w_g = N^2k/(Un^3).$$

Hence for a ridge centred at $(x, z) = (0, 0)$ the ray path of a packet will lie along the straight line,

$$Z = (f/N)(R_o^2 - 1)^{3/2}X,$$
$$\text{where} \quad (X, Z) = (x/L, z/L). \tag{10a}$$

Likewise the phase line for the first downstream minimum is delineated by

$$Z = -\{(f/N)(R_o^2-1)^{1/2}\}[X - \gamma]$$
$$\text{where} \quad \gamma = (3\pi/2). \tag{10b}$$

Thus, the flow structure closest to incipient wave-overturning will prevail at the intersection of the ray path and the first downstream minimum of u, i.e., at

$$X^* = \gamma/R_o^2,$$
$$Z^* = \gamma(f/N)(R_o^2-1)^{3/2}/R_o^2. \tag{10c}$$

(For a packet with a lateral scale corresponding to R_o and under typical ambient atmospheric conditions the location of this intersection varies continuously from being above the crest at a height of 4.5 km for $R_o \sim 10$ to being at the surface and 450 km downstream for $R_o \sim 1$.)

Now consider the amplitude of the perturbed flow structure at (X^*, Z^*). Wave overturning due to a packet centred at the R_o-scale and with a spectral band-width (ΔR_o) will be favoured if both the amplitude of the dominant modes and their degree of coherence across the band is large. These requirements correspond to:

large values for the perturbation to the incident flow, i.e., large values of

$$(u^*/U) = FR_o/\{R_o^2 - 1\}^{1/2}, \tag{11a}$$

small values for amplitude variation across the band, i.e., of

$$\frac{\partial(u^*/U)}{\partial R_o}(\Delta R_o) = -F/\{R_o^2-1\}^{3/2}(\Delta R_o), \qquad (11b)$$

and little spatial variation of (X^*, Z^*) relative to the packet's predominant horizontal and vertical wavelengths, i.e., low values of

$$\left\{k\frac{\partial(\mathrm{L}X^*)}{\partial R_o}\right\} = (9\pi/2)(R_o)^{-3}, \qquad (11c)$$

$$\left\{n\frac{\partial(\mathrm{L}Z^*)}{\partial R_o}\right\} = (9\pi/2)(R_o)^{-3}. \qquad (11d)$$

Conditions (11a–11d) serve to pick out and illustrate the properties of two particular wave packets. Firstly *quasi-inertial horizontally-propagating* packets are linked with: large amplitude; a rapid amplitude decrease across the band; and weak coherence. The large amplitude betokens potential nonlinearity and contraction of the upslope width (see previous sub-section) whilst the other effects tend to counter overturning.

Secondly for a packet of *essentially vertically propagating, hydrostatic buoyancy modes*, i.e., a packet characterized by $R_o \sim 10$, the waves are of almost uniform amplitude and highly coherent. For a broader ridge of the same height the orographic forcing of these particular modes, and hence their efficacy for wave overturning, will be less. For example consider an isolated bell-shaped ridge, i.e.,

$$\eta(X) = H/(1+X^2).$$

For a ridge of half-width corresponding to $R_o = R_o^*$

$$\eta(0) = (H/R_o^*)\int_0^\infty \exp\{-R_o/R_o^*\}\,\mathrm{d}R_o.$$

Integrating across only the "buoyancy-wave" spectral band $[(R_o\text{-}\Delta R_o/2), (R_o+\Delta R_o/2)]$ with say, $(R_o \sim 10, \Delta R_o \sim 1)$, the amplitude associated with these waves can be shown to be proportional to,

$$2\exp\{-R_o/R_o^*\}\sinh[\tfrac{1}{2}\Delta R_o/R_o^*]. \qquad (11e)$$

It follows that, as the width of the isolated ridge changes from $R_o^* \sim 10$ to $R_o^* \sim 1$, there is an order of magnitude decrease in the composite amplitude of the forcing for the coherent buoyancy waves. In effect linear theory suggests that the potential for overturning due to directly forced coherent buoyancy waves is a substantially reduced for intermediate scale terrain.

2.3. *The isentropic non-linear flow system*

In the limit of hydrostatic flow over isentropic orography there are distinct conceptual and mathematical advantages in formulating the governing equations in a θ-coordinate framework. For the Boussinesq system, the resulting nonlinear equations for the perturbation variables take the form,

$$Lu - fv = -m_x, \qquad (12a)$$

$$Lv + fu = 0, \qquad (12b)$$

$$Lh + M_{\theta\theta}u_x = 0, \qquad (12c)$$

with

$$m_\theta = -(g/\Theta)\,z, \qquad h = m_{\theta\theta}. \qquad (12d)$$

The x-subscripts refer to a horizontal derivatives along an isentropic surface and now

$$L = \frac{\partial}{\partial t_\theta} + u\frac{\partial}{\partial x_\theta}$$

is the (time-dependent) material derivative in this framework. The variable M is the system's equivalent of the Montgomery streamfunction, and is given by,

$$M = \{p/\rho_0 - (g\theta/\Theta)\,z\}.$$

Here ρ_0 and Θ refer to a reference isentropic state, and p is the departure of the pressure away from this state. M has been further partitioned such that,

$$M = (\mathcal{M} + m),$$

where the two components refer respectively to the upstream value and the deviation therefrom. In terms of this partition h is a measure of the isentrope separation. Likewise z now refers to the displacement of an isentrope away from its upstream elevation Z.

Finally, we note that for isentropic terrain the lower boundary is

$$z(x, \theta_{\text{bottom}}) = \eta(x). \tag{13}$$

Several previous orographic flow studies have adopted an isentropic (or related) coordinate system (Krishnamurti, 1964; Eliassen and Raustein, 1970; Eliassen and Rekustad, 1971; Eliassen and Thorsteinsson, 1984; Davies and Horn, 1988; Smith, 1988). The utility of, and the problems posed by, such systems are discussed in Shapiro (1974) and Hsu and Arakawa (1990). The system (eqs. (12–13)) forms the basis of the nonlinear numerical model that will be used later to simulate the flow response in the intermediate domain of (R_o, F) parameter space.

Here in conformity with the stipulated objective for this section we consider some further theoretical aspects. A steady state solution of the set of eqs. (12–13) in the semi-geostrophic limit, i.e., eq. (12a) replaced by the geostrophic relation $fv = m_x$, was derived by Davies and Horn (1988) for flow over bell-shaped isentropic terrain, i.e.,

$$\eta(x^*) = h/\{1 + x^{*2}\}$$
$$\text{where} \quad x^* = (x/L). \tag{14}$$

The spatial pattern of the across-ridge velocity component was shown to be,

$$u(x^*, \theta) = U\{1 - (R_o F)(\delta^2 - x^{*2})/(\delta^2 + x^{*2})^2\}^{-1}$$
$$\text{where} \quad \delta = \{1 + (R_o F)\,\theta\}. \tag{15}$$

Thus, it takes the forementioned form of an evanescent structure in the vertical, a slackening of the wind up- and down-stream of the ridge, and a speed-up and strengthening of the stratification at the crest. The intensity of these features intensify as $R_o F$ increases and become singular at the crest for $R_o F = 1$. Our interest centres on the form of the physical transition that presages this mathematical breakdown.

A theoretical framework for examining this transition was set out in Davies and Horn (1988). The residual flow forced by the semi-geostrophic response is isolated by decomposing the full flow field in the form,

$$(u, v, m) = (u_s, v_s, m_s) + (u', v', m'), \tag{16}$$

where the subscript s and the "prime notation" refer respectively to the semi-geostrophic and residual flow components. The linear features of the residual flow are then determined by the differential equation,

$$[(\mu U/f)^2 (u_s/U)^3 m'_{\theta\theta}]_{xx} + \mu^2 m'_{\theta\theta} + m'_{xx}$$
$$= -\tfrac{1}{2}(u_s^2)_{xx}$$
$$\text{with} \quad \mu^2 = (f^2/\mathcal{M}_{\theta\theta}), \tag{17}$$

which is a variant of the standard steady-state transmission equation for inertia-buoyancy waves. There is a modification of the refractive index due to the non-uniform structure of the semi-geostrophic flow field, the term involving u_s^3, and in addition the semi-geostrophic flow provides a source of forcing (the term involving u_s^2) for the residual flow.

The equation is subject to the boundary conditions,

$m'_\theta = 0$ at the lower boundary, and (18a)

either m'_θ tends to zero,
or a radiation condition prevails as θ tends to infinity. (18b)

It follows from eqs. (15 and 17) that the forcing is non-zero at the lower boundary and decays exponentially in the vertical. Hence the solution will take the general form,

$$m' = m'_1 + m'_2.$$

Here m'_1 and m'_2 satisfy respectively the inhomogeneous and homogeneous forms of eq. (18), with the boundary conditions satisfied by

$$(m'_1)_\theta = -(m'_2)_\theta$$

at the lower boundary, and m'_1 and m'_2 separately satisfy the pertinent form of the upper boundary condition.

Consider now the ageostrophic forcing term due to the balanced flow as $R_o F \to 1$. At this forcing, (the r.h.s. of eq. (17)) can be written in the form,

$$-\tfrac{1}{2}(u_s^2)_{xx} = (f^2 R_o^2)\,\chi,$$
$$\text{where} \quad \chi = [-\tfrac{1}{2}(u_s^{*2})_{x^*x^*}].$$

Fig. 2 shows the surface distribution of the non-dimensional variable χ for a range of values for $R_o F$. On the basis of the above formula and the displayed distributions it can be inferred that there are two salient ingredients to the forcing: its spatial structure corresponds to a scale contraction by a factor of ~ 4 relative to that of the terrain with only a slight dependence upon $R_o F$; its amplitude increases rapidly and is proportional to $\sim R_o^2(1 - R_o F)^{-3}$. It follows that for $R_o F$ in the range [0.25, 0.75] there is substantial forcing on scales such that $(Uk/f) \gg 1$, corresponding in effect to the scale of inertia-buoyancy waves. It follows that the m_2' component of the residual flow will be linked with such propagating waves.

This entire process constitutes one putative and particularly simple example of "geostrophic adjustment". In essence for flows characterized by $R_o \sim (\frac{1}{4} - 1_-)$ and $(R_o F) \sim 1_-$, there is a steady spatially well-defined geostrophic forcing of ageostrophic flow in the vicinity of the crest, and this forcing is compatible with the generation of inertia-buoyancy waves.

2.4. *Synthesis of theoretical considerations*

The speculative inferences drawn in the previous sub-sections suggest that several processes might influence the pathway to regime transition in the intermediate domain of (R_o, F) parameter space.

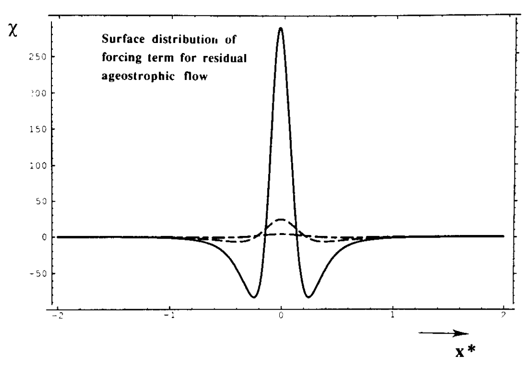

Fig. 2. Surface distribution of the semi-geostrophic forcing of residual ageostrophic flow for flow over a bell-shaped ridge. The function displayed is the non-dimensional χ component of the forcing, and it is shown as a function of the non-dimensional spatial scale $x^* = x/L$ for $R_o F = 0.25$, 0.5 and 0.75 (correponding respectively to the short-dashed, long-dashed, and solid lines).

It was indicated that a broadening of a ridge of stipulated height, corresponding to a decrease of R_o whilst keeping F constant, will reduce the amplitude of the vertically propagating almost non-dispersive buoyancy waves and concomitantly decrease their efficacy to effect a wave overturning. Furthermore for $R_o > 1$ the strong direct forcing of inertia-buoyancy waves was offset by their highly dispersive properties. However for $R_o \sim 1_+$ the leeward train of low-level near-inertia waves has a large amplitude. Finally for $R_o < 1$ the breakdown of the balanced flow response was linked to the possible generation of geostrophically forced inertia-buoyancy waves.

These inferences are explored further by undertaking nonlinear flow simulations with a numerical model.

3. Framework for the numerical simulations

3.1. *The numerical model*

From a modelling perspective the co-existence of a range of flow features with differing space-time characteristics places severe and often incompatible demands upon the design of an appropriate numerical model. This is true for the intermediate domain of (R_o, F) parameter space. The potentially significant flow features include: wave-overturning for $R_o \gg 1$; the small vertical scale of $R_o \to 1$ features (either rapid evanescence for $R_o \sim 1_-$, or short vertical wavelengths for $R_o \sim 1_+$); and the possible occurrence of fine-scaled buoyancy waves within a quasi-balanced flow for $R_o \ll 1$. Explicit consideration of wave overturning would require a non-hydrostatic model and very high horizontal resolution. Also the representation of near-inertial features would require high vertical resolution and an extended spatial domain to the lee, and simulating the adjustment process requires adequate simultaneous representation of both the synoptic/sub-synoptic balanced flow and the meso α/β scale inertia-buoyancy waves.

Here the focus is to explore the pathway toward regime transition. Hence the rationale adopted is to exclude a priori an explicit consideration of wave overturning, invoke the hydrostatic assumption and adopt an isentropic vertical coordinate. This framework, coupled with a high horizontal resolution, will help capture the rich vertical structure of the near-inertial signals and the essence of the adjustment process, but it will be less accurate in representing steep isentropic slopes.

The numerical model is based upon the non-linear hydrostatic Boussinesq system cast in the isentropic framework that was introduced earlier (see eqs. (12)). The lower boundary condition constrains the terrain to be isentropic (eq. (13)) and the upper boundary is taken to be a θ surface with an unperturbed pressure field, i.e.,

$$m(x, \theta_{\text{top}}) = 0. \tag{19}$$

For the numerical simulations an explicit weak horizontal diffusion scheme for momentum is incorporated to alleviate the effects of down-scale energy cascade, and at the lateral boundaries and in the upper part of the domain marginal zones are introduced where the flow is relaxed toward an externally prescribed structure (Davies, 1983).

The numerics of the model is based upon second-order finite-differences in space and time. The spatial grid is defined by $\{x = j(\Delta x), \theta = k(\Delta\theta)_k\}$ with typically (500×90) points of equal spacing, Δx, in the horizontal and a stretched system defined by $(\Delta\theta)_k = 0.6 \exp^{\{k/20\}}$ in the vertical with $k = 1$ denoting the surface. The relaxation zones occupies 6 grid points at the lateral boundaries and the 8 uppermost levels. In the horizontal the lattice is that of the Arakawa C-grid (Mesinger and Arakawa, 1976). For the momentum equations (eqs. (12a, b)) the finite-difference for the material derivative is based upon the vector invariant form (Sadourny, 1975) and the leapfrog time scheme is supplemented by a weak Asselin filter. For the time development of the isentropic separation, i.e., the h of (eq. (12c)), the material derivative is approximated by a positive definite algorithm (Smolarkiewicz, 1984). In the vertical the variables (u, v, h, m) are colocated, and the second order differencing of eq. (12d) links every vertical column of discrete h and m values via a tri-diagonal matrix. With the prescribed boundary conditions (eqs. (13) and (17)) the inversion of the updated h values to obtain the new m values is readily accomplished by sequentially sweeping up and down each vertical column.

Further details of the model are to be found in Trüb (1993).

3.2. *Design of simulation experiments*

Series of numerical experiments were conducted to determine the nature of the flow over a Gaussian shaped ridge,

$$\eta(x) = H \exp\{-(x/L)^2\}. \tag{20}$$

For each experiment, the terrain together with the externally specified upstream flow structure serve to establish the (R_o, F) values of the simulation, and settings for the experiments are arranged to span the "intermediate domain" of (R_o, F) space.

The parameters L, U, and N were set respectively at 100 km, 10 ms^{-1} and $10^{-2}\,\text{s}^{-1}$, and the coefficient for the isentropic momentum diffusion assigned a value yielding an e-folding time of 20 min for $(2\,\Delta x)$ waves. Different values of R_o and F were achieved by selecting different values for the Coriolis parameter f and ridge height H.

For each simulation the initial conditions (and the state to which the flow is guided in the relaxation zones) were set to correspond to a geostrophically balanced uniform flow $\boldsymbol{v} = (U, 0, 0)$ of uniform stratification (N) so that,

$$\mathcal{M} = -fUy - (g/\Theta N)^2\,\theta^2. \tag{21}$$

Every simulation was in two phases. First a period of orogenesis defined by

$$z_{\text{bottom}} = \eta(x)\,\alpha(t), \tag{22}$$

with $\alpha(t)$ transiting smoothly from zero to unity, followed by a time integration until the flow became quasi-steady.

Diagnosis of the flow structures was undertaken by inspecting: the primary variables of velocity (u, v) and isentropic displacement (z); and four secondary variables viz. the divergence $D = (u_x)$ on a θ-surface, the parameter Φ defined by the integral of $\{(\frac{1}{2}u^2)_x\,\eta(x)\}$ along the terrain, the isentropic potential vorticity $P = \{(v_x + f)/(-M_{\theta\theta})\}$, and the Bernoulli function $B = \{\frac{1}{2}(u^2 + v^2) + M\}$. The rationale for examining these secondary variables is as follows. The D-field provides a dynamical indicator of the occurrence, amplitude and the ray path of the buoyancy waves, and the measure (Φ) is a sensitive one-parameter measure of the buoyancy wave activity. Further the potential vorticity is conserved for the continuous, non-diffusive form of the flow system and it has an uniform value in the initial field. Thus any departure from that uniform value reflects the defects of the finite-difference scheme and/or the influence of the explicit pseudo-diffusion. Likewise for steady state flow the material derivative of the Bernoulli function is conserved.

3.3. A model validation

The principal objective of the present study is to examine the pathway toward a regime change within parameter space. This change is manifest by the occurrence of for example wave-overturning or upstream flow blocking, but these processes can not be considered explicitly in our hydrostatic model. Nevertheless, it is important that the approach to transition is represented adequately by the model and also appropriate to assess its behaviour at and beyond the transition. This can be done in the non-rotating ($f=0$) limit since results from non-hydrostatic simulations and analytical solutions are available.

Fig. 3 pertains to an airstream above finite-amplitude ($F=0.5$) bell-shaped terrain. It shows the flow structure derived after an extended time integration of the numerical model superimposed upon the corresponding steady state nonlinear hydrostatic analytical solution (Long, 1953; Lilly and Klemp, 1979). The numerical model captures the quantitative features of the upward propagating nonlinear buoyancy wave but there is a tendency to underestimate the steepening of the upslope segment of the wave pattern above the terrain.

Consideration of the analytical solution for irrotational hydrostatic flow over a finite-amplitude bell-shaped ridge (Miles and Huppert, 1969; Lilly and Klemp, 1979) shows that the steepening intensifies as F increases with an accompanying moderate increase in the surface drag, and eventually an isentrope attains a vertically alignment at $F=0.85$. Thereafter non-hydrostatic numerical models indicate that, following the occurrence of wave-breaking, there is a much more rapid increase of the drag. Fig. 4 displays the variation of the surface drag with F as obtained from simulations with the present model and as derived analytically with a perturbation approximation (Miles and Huppert, 1969). Both evaluations have been normalized by the estimate of the drag derived from linear theory. The substantial degree of agreement indicates that for this particular configuration, the numerical model not only mimics the main flow features adequately but also accurately demarcates the location of the regime transition.

Note also that for this flow setting, the regime transition is marked physically by the onset of

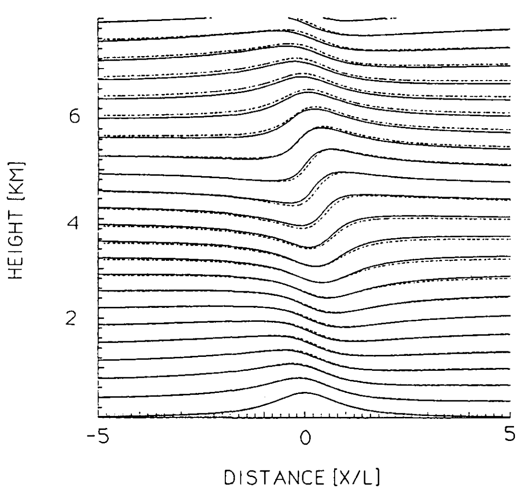

Fig. 3. The quasi-steady isentropic patterns for the non-rotating setting with $F=0.5$ obtained with the numerical model (solid lines) and the analytical solution of the hydrostatic form of Long's equation (dashed) after Lilly and Klemp (1979).

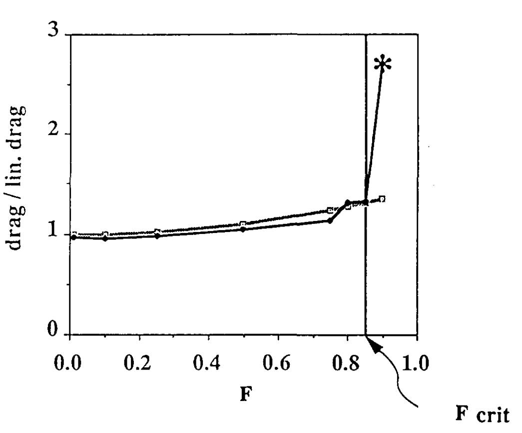

Fig. 4. The normalized surface drag in the hydrostatic non-rotating limit of flow over a bell-shaped ridge shown as a function of F. The two curves pertain to that derived for the analytical solution (light shading) after Miles and Huppert (1969) and the values computed for the non-linear numerical model (solid). (Note that for $F > F_{\text{crit}}$ the numerical simulation did not attain a steady state.)

convective instability, whereas in the model this instability is excluded using a positive definite algorithm in the prediction equation (eq. (12c)) for the inverse of the static stability. Thus, in the numerical model, wave-overturning is replaced by a marked increase in diffusive effects at the steep slope, and this in turn can serve as a source for buoyancy waves with an accompanying enhancement of the surface drag. The results lend credence to our approach.

For the more general simulations reported in the next section the detection of regime transition will be monitored using measures of both the buoyancy wave activity and diffusive effects as diagnostic parameters. In the customary fashion a check on the robustness of these simulations was also undertaken by conducting the experiments with different values for both the horizontal and the vertical resolution.

4. The flow response in the intermediate domain of (R_o, F)

In this section, we discuss in turn the nature of the flow response for the three Rossby Number settings of $R_o = (3, 1, \frac{1}{4})$, each for a range of values of F.

4.1. The $R_o = 3$ setting

At this value of R_o, considerations based upon linear theory indicate that rotational effects are still comparatively weak, e.g., eq. (10a) indicates that the slope of the ray path will be reduced to only $\sim 20(f/N)$. Thus the response is expected to be qualitatively akin to those illustrated for the non-rotational limit in Subsection 3.3. This is borne out in Figs. 5 and 6 which show the isentropic displacement field, the divergence pattern, and perturbation across-ridge and the along-ridge velocity components for respectively the quasi-linear ($F = \frac{1}{40}$) and the nonlinear ($F = \frac{3}{4}$) settings. To facilitate comparison of the two cases and in particular to highlight the influence of non-linear effects the amplitude of the fields for the quasi-linear case have been magnified by a factor of 30.

Inspection of the two cases shows the nonlinear steepening of the upslope portion of the isentropes above the terrain, and also a strengthening and slight downstream displacement of the wind maximum on the lee slope. For both settings there is evidence of a weak quasi-inertial scale wave-train near the surface.

4.2. The $R_o = 1$ setting

Figs. 7 and 8 display the same fields as in Subsection 4.1 but now for respectively $F = \frac{1}{40}$ and 1. (Again for comparison purposes the response in the first case has been magnified, now by a factor of 40). For the small F-case the main differences, relative to the response at $R_o = 3$, are in line with our earlier consideration of linear wave theory. The differences are a shallower inclination to the buoyancy wave train (c.f. eq. (10a)), a decrease in its strength (c.f. eqs. (11e)), an enhancement of the quasi-inertial signal (c.f. discussion following eqs. (11a–d)), and an increase in the across-ridge asymmetry of the D-field indicative of a quasi-geostrophic component to the flow response (c.f. eq. (15)).

Nonlinear effects (c.f. Figs. 7, 8) again induce a steepening of the upslope portion of the buoyancy waves above the terrain and this is accompanied by a substantial downstream shift of the isentropic upwelling on the lee slope. There are two further novel features to the response. Firstly, there is a marked asymmetry in the length scales associated, respectively, with the up- and down-welling segments of the lee-side low-level quasi-inertial waves, resulting in sharpened crests and smeared troughs. Secondly, ray paths with buoyancy-wave characteristics emanate from the vicinity of the aforementioned low-level downstream crests into the interior of the domain. These additional wave trains track at a steeper angle than the train from the mountain ridge itself and have an appreciable amplitude. Indeed, the strength of the divergence-field of the ray path emanating from the first downstream crest is comparable to that of the ray path from the ridge.

An indication of the evolution, and insight to the dynamics, of the cusp structures can be gleaned from Fig. 9. It shows a time-sequence of the isentropic pattern superimposed upon the D-field for the $F = 1$ simulation. The display captures the sequential formation of the cusp-like crests and the accompanying formation of the forementioned ray paths. The co-occurrence and co-location of the cusp-like features and the source of buoyancy waves is consistent with the nonlinear modification of the near-inertial waves such that the smaller spatial structure of the crests serve as a source of

Tellus A/47/4-9

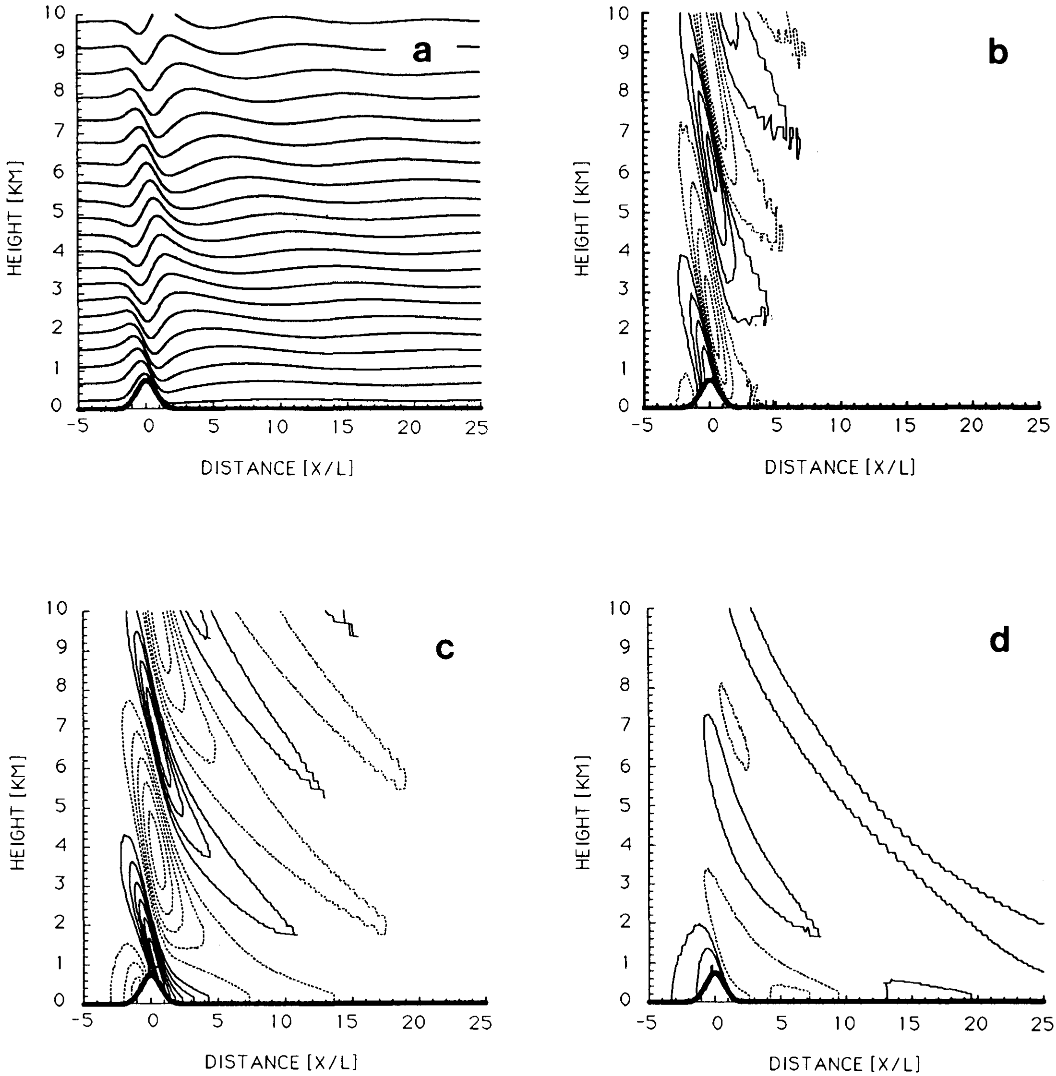

Fig. 5. Quasi-steady state orographic flow response for $R_o = 3$ and $F = \frac{1}{40}$. Displayed are the cross-sectional distribution of (a) the isentropic displacement field, (b) the divergence pattern, and (c, d) the perturbation across-ridge and the along-ridge velocity components (isoline increments are at intervals of 1 ms^{-1}). For later comparison the amplitudes of this quasi-linear response have been magnified by a factor of 30.

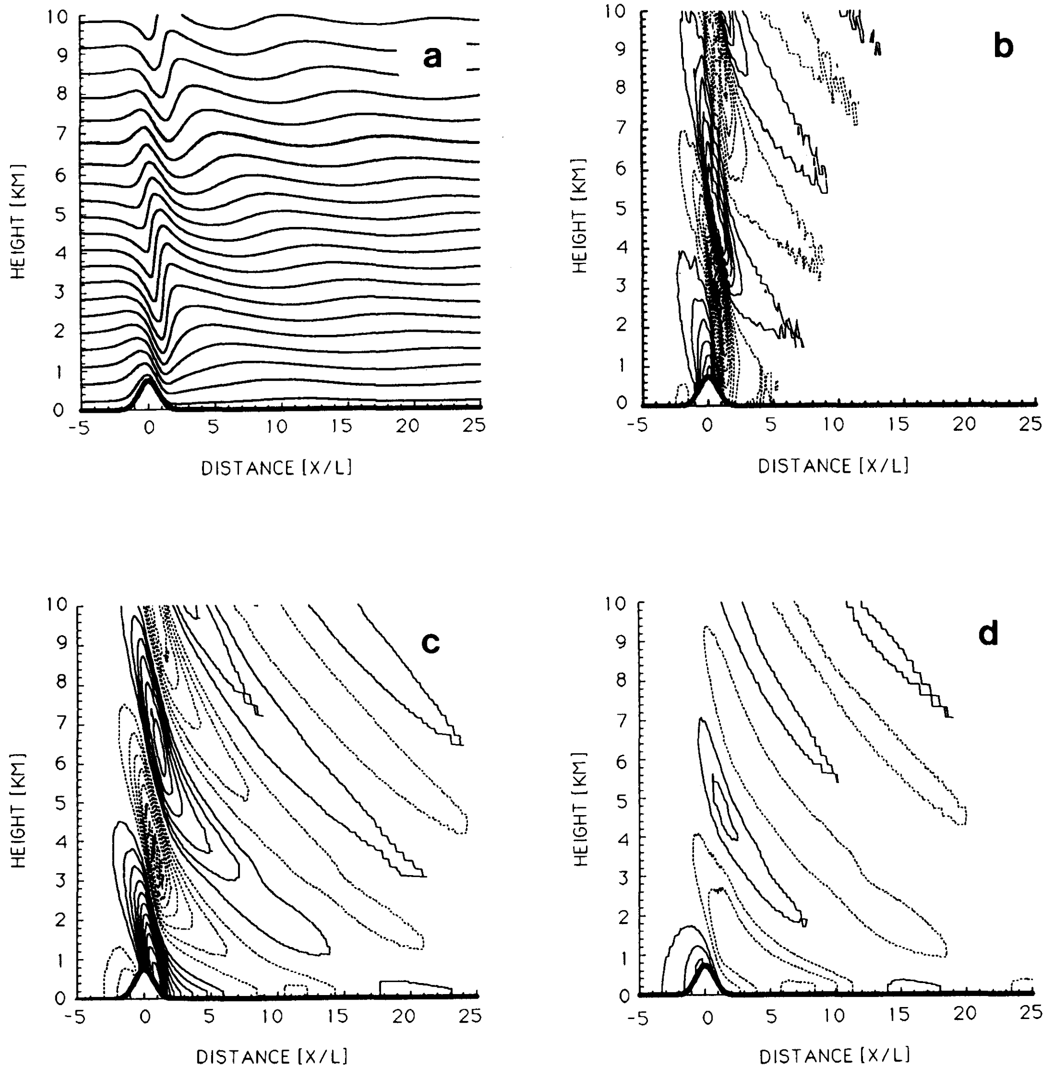

Fig. 6. Quasi-steady state orographic flow response for $R_o = 3$ and $F = \frac{3}{4}$. (Display as for Fig. 3 but with no amplification.)

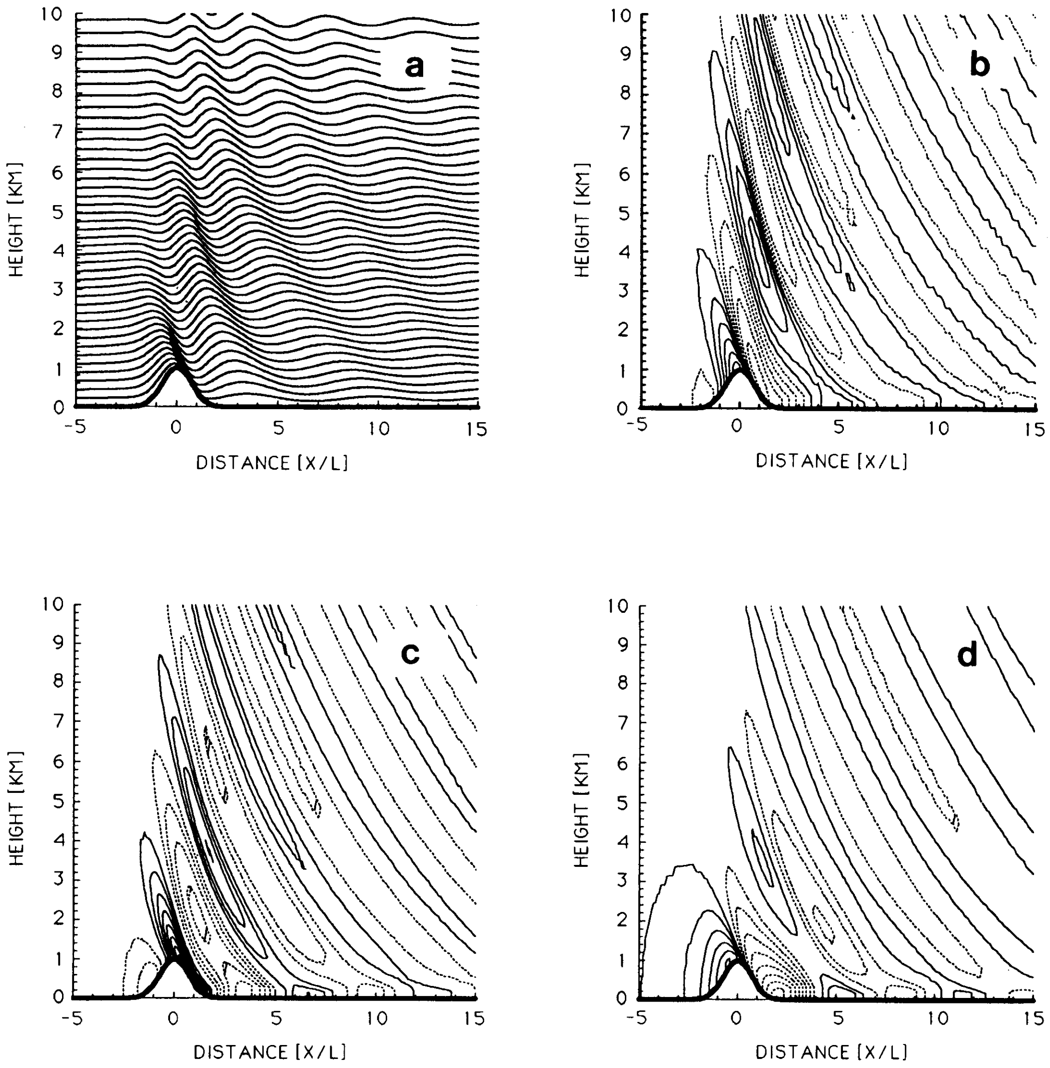

Fig. 7. Quasi-steady state orographic flow response for $R_o = 1$ and $F = \frac{1}{40}$. (Display as for Fig. 3, but with the response magnified by a factor of 40.)

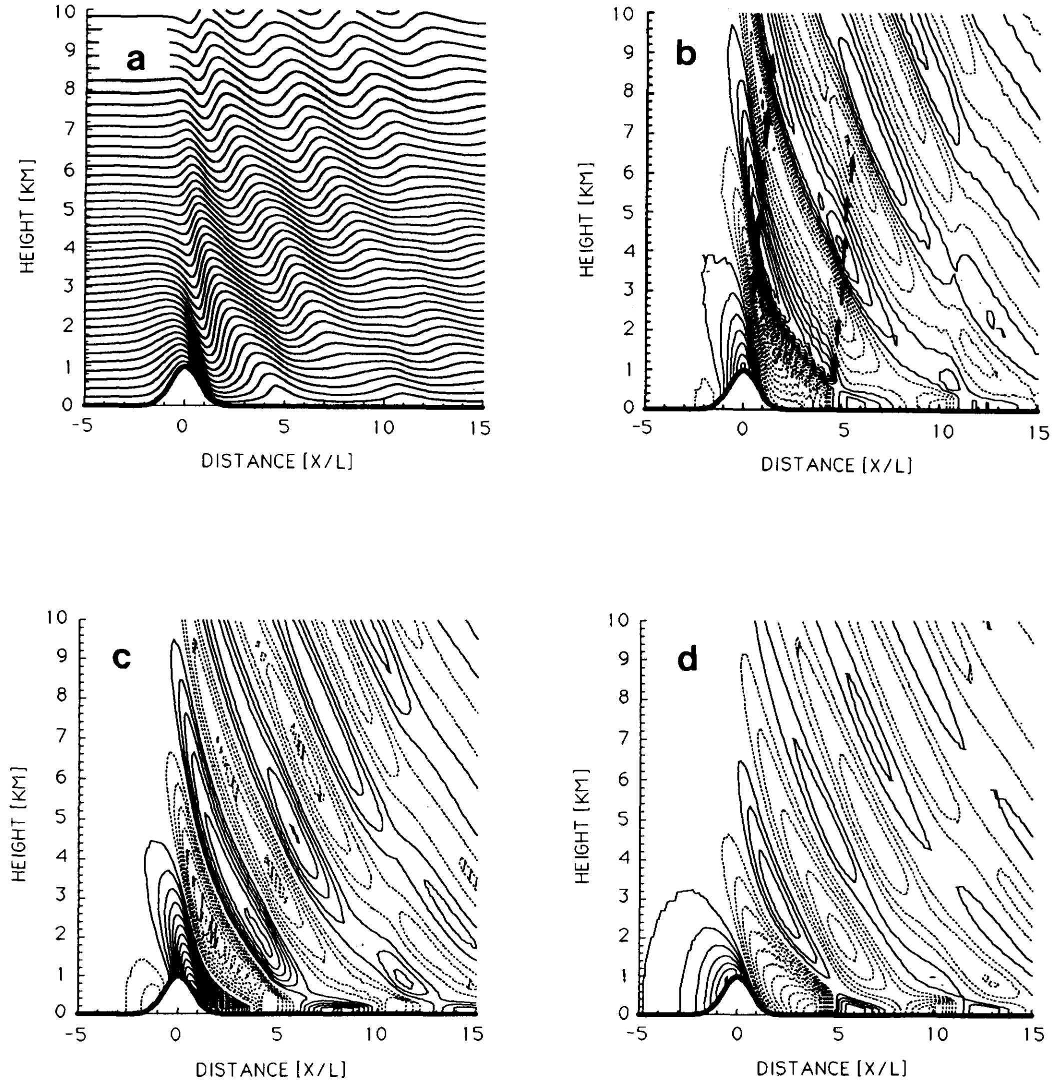

Fig. 8. Quasi-steady state orographic flow response for $R_o = 3$ and $F = 1$. (Display as for Fig. 3 but with no amplification.) The sequence of arrows demark the ray paths of the buoyancy waves tracking away from the ridge (long arrows) and the cusp region (shorter arrows).

buoyancy waves. In a different context, Durran (1992) showed that nonlinear finite amplitude buoyancy waves could themselves induce smaller scale buoyancy waves. In the present case the upward leakage of energy into the interior can have two concomitant repercussions. Firstly it can serve to offset the in-situ tendency for cusp formation and thereby permit a possible equilibration between the effects of scale contraction and buoyancy wave radiation. Secondly it can deplete the energy associated with the low-level near-inertial ray path and thereby reduce the potential for cusp formation further downstream.

Evidence to support these purely qualitative

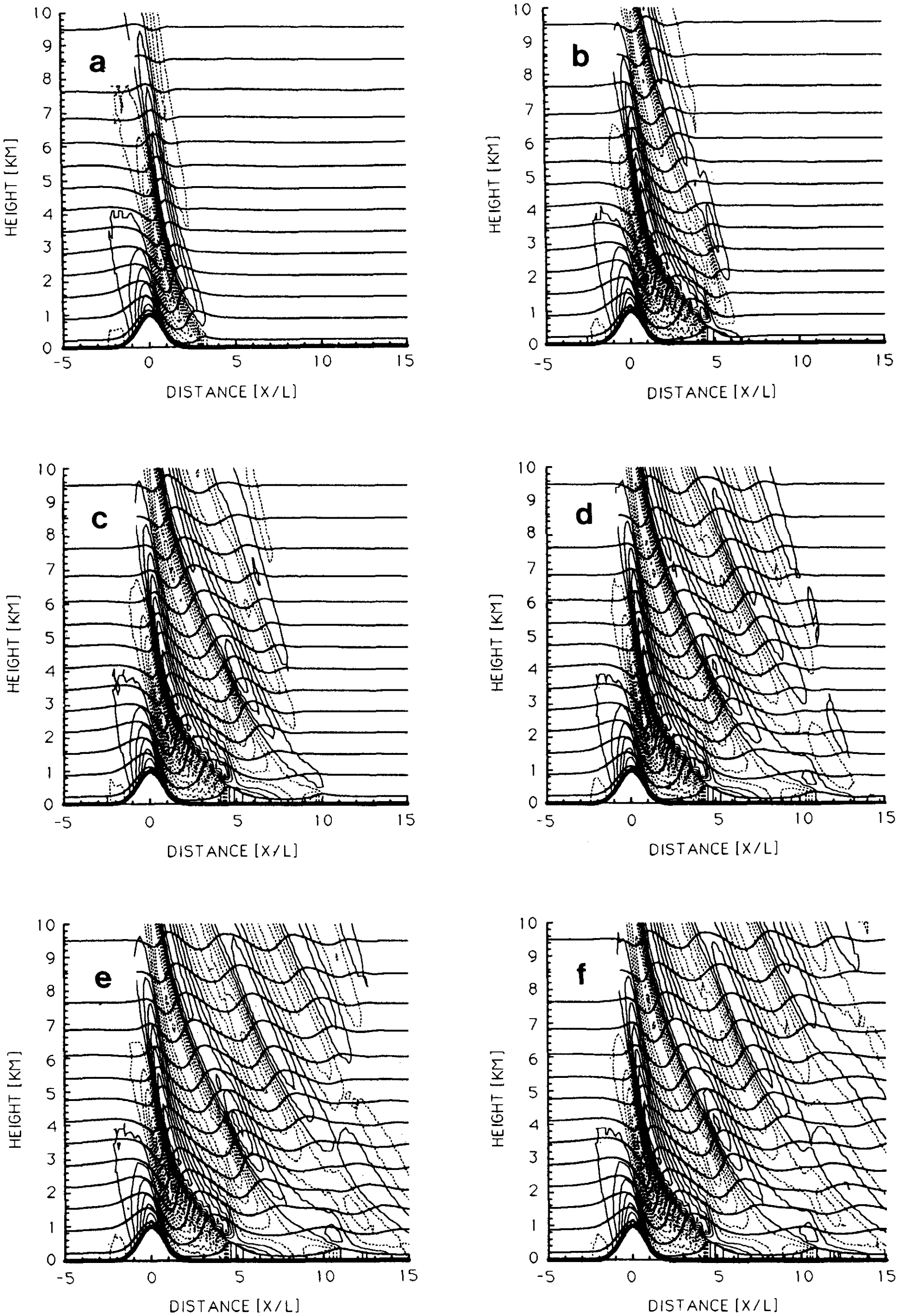

Fig. 9. A time-sequence of the coss-sections for the isentropic displacements (bold solid lines) and the divergence field (light solid and dashed contours) for the setting $(R_o, F) = (1, 1)$. Panels (a–f) correpond respectively to the dimensional times of ~6, 17, 28, 39, 50, and 60 h.

inferences is provided in Fig. 10. A scaled measure of the steady-state near-surface values of the scaled nondimensionalised velocity components, viz. $(u^*, v^*) = (u', v')/(UF)$, is shown for simulations undertaken with $F = 0.25$, 0.5, 0.75, and 1. Nonlinear effects are evident with the extremae being displaced downstream as F increases. Note however that, unlike the other extremae, the amplitude of the first downstream u^* minimum (i.e., the first lee-side near-inertial wave crest) does not exhibit an F dependency, whilst the amplitude of subsequent extremae decrease leeward. This lends credence to the aforementioned equilibration hypothesis. Furthermore the small values of u^*F (values ranging from 0.125-to-0.5) demonstrate that the formation of buoyancy waves at the first downstream minimum is not linked to a flow-stagnation phenomenon.

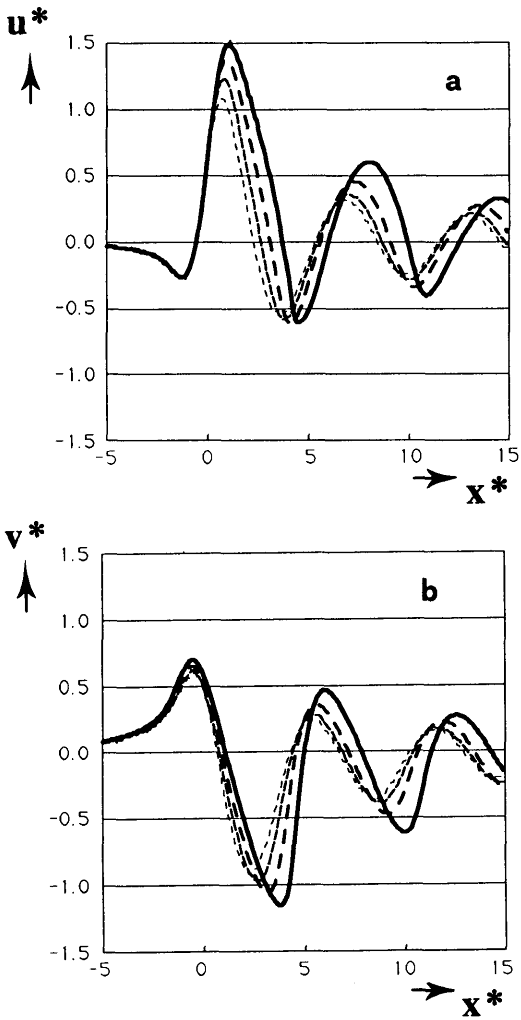

Fig. 10. Spatial distribution of the steady-state near-surface velocity components for simulations undertaken with $R_o = 1$ and with $F = 0.25$, 0.5, 0.75, and 1 (continuity of the lines increases with F). The displayed fields are the rescaled non-dimensional measures $(u^*, v^*) = (u', v')/(UF)$.

4.3. The $R_o = 1/4$ setting

Figs. 11, 12, and 13 relate to the response for $F = (0.01, 1, 2)$ and show as before the isentropic displacement, the D-field, and the perturbation across- and along-ridge flow components. (Here the amplitude of the response for the $F = 0.01$ case has been magnified by a factor of 200.)

At this value of R_o the rotational effects are expected to be strong. The semi-geostrophic response prevails for $R_o F \ll (\pi^{1/2}/2)$ (Pierrehumbert, 1985) and Fig. 11 shows the characteristic evanescent response. For $F = 1$ the semi-geostrophic response remains dominant but there is some evidence (see in particular Fig. 12b) of two non-balanced flow components, a steeply-inclined inertia-buoyancy wave train, and a low-level near-inertial wave component. At $F = 2$ (Fig. 13), the amplitude of both these non-balanced structures has increased substantially and become prominent features of the isentropic displacement and divergence fields. Their combined effect modifies the balanced flow signal to produce a strong low-level wind on the upper lee slope and a large amplitude and relatively sharp wave crest above the lower portion of the slope. In this case too there is some indication of a ray path emanating from a downstream crest of the near-inertial wave.

Figs. 14, 15 serve as indicators of the non-balanced wave features. In Fig. 14 the suitably magnified isentropic distribution for the $F = 0.01$ case is superimposed upon that for the $F = 2$ setting. This comparison confirms the lack of appreciable direct orographic forcing of buoyancy waves (c.f. eq. (11e)) and highlights the non-linearly-generated features of the $F = 2$ field. In Fig. 15, a measure (Φ) of the buoyancy wave activity, defined by the integral of $\{(\frac{1}{2}u^2)_x\, \eta(x)\}$ evaluated along the terrain, is displayed as a function of $R_o F$ for three specific values of R_o (we note in passing that Φ equates to the drag in the non-

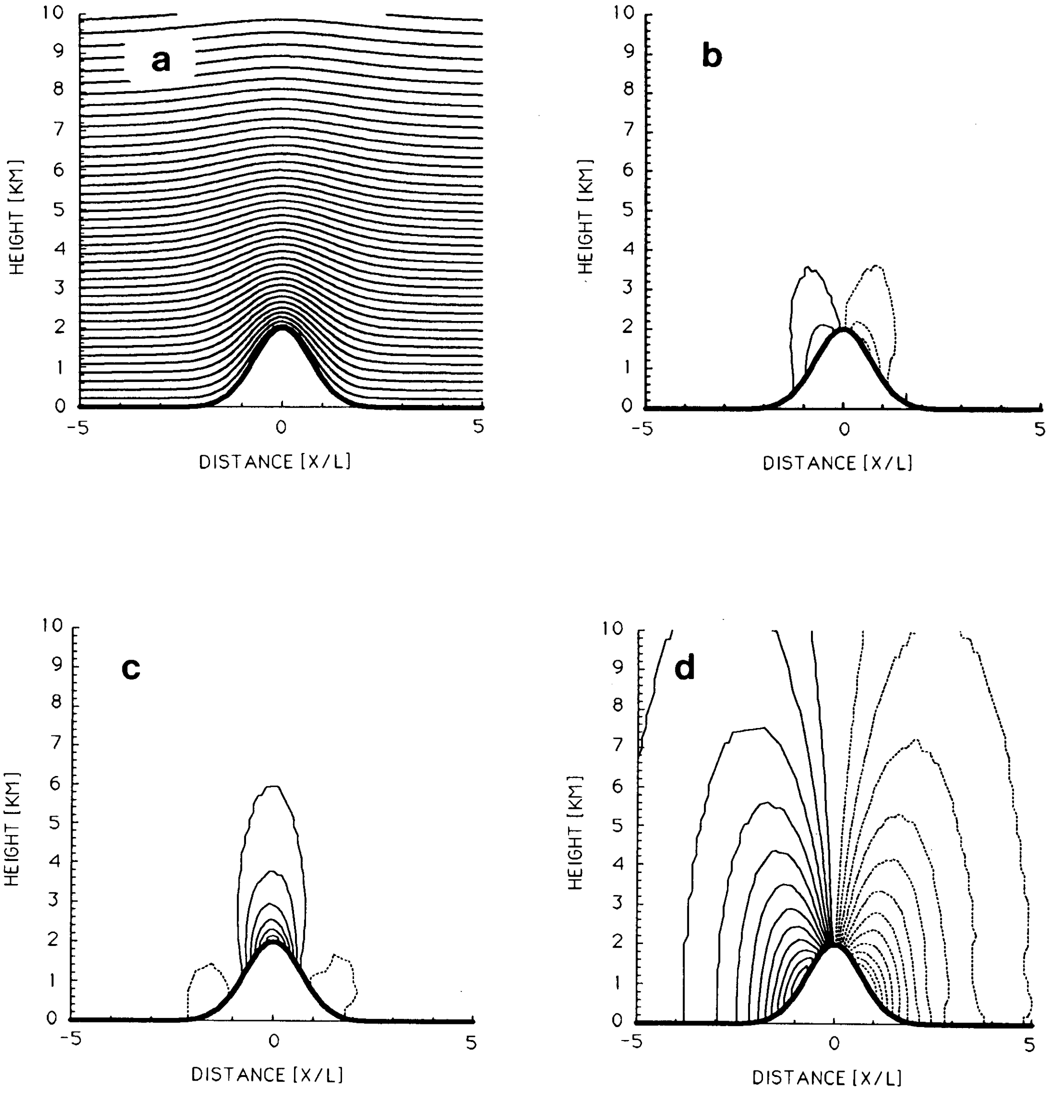

Fig. 11. Quasi-steady state orographic flow response for $R_o = 0.25$ and $F = 0.01$. (Display as for Fig. 3, but with the response magnified by a factor of 200.)

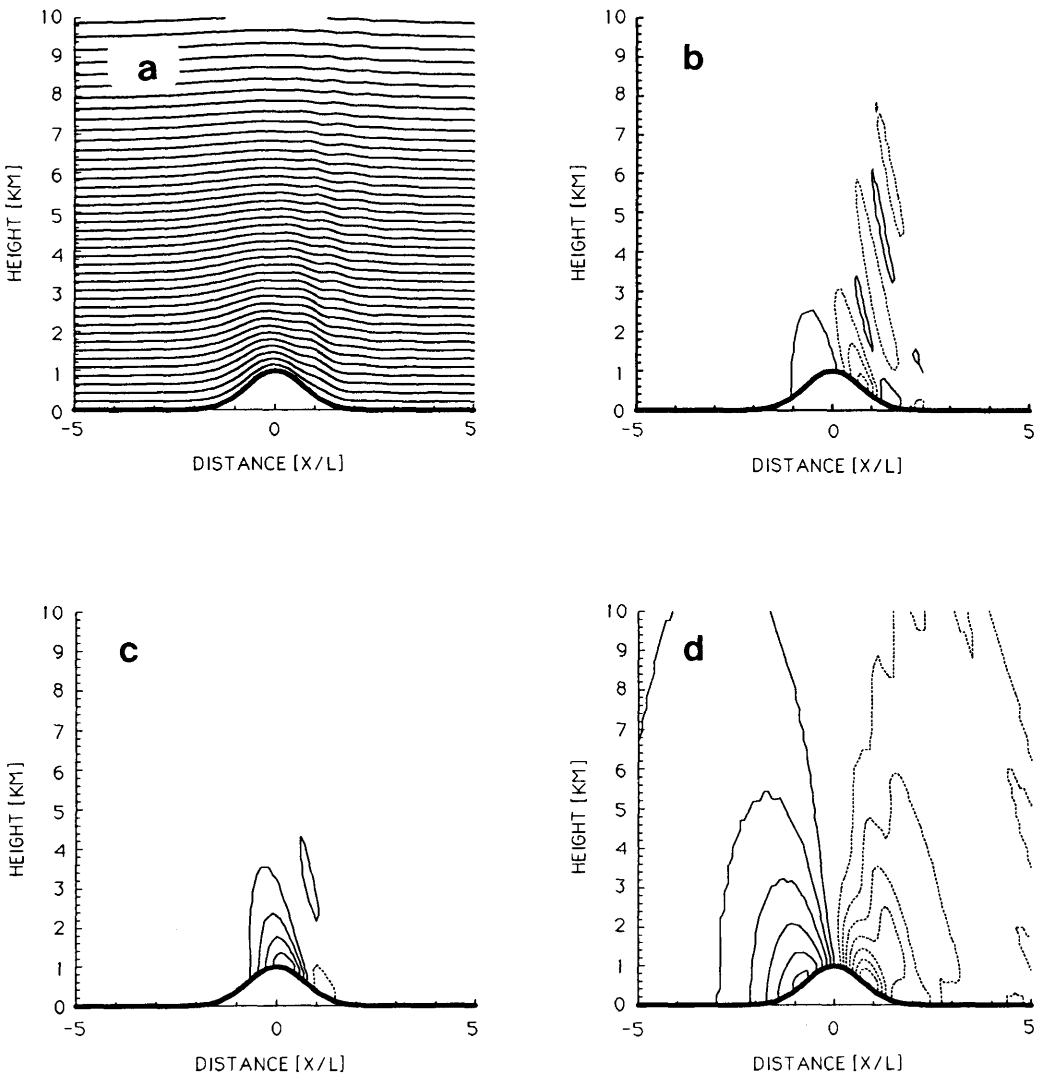

Fig. 12. Quasi-steady state orographic flow response for $R_o = 0.25$ and $F = 1$. (Display as for Fig. 3 but with no amplification.)

rotating limit, and that for purely balanced flow, $\Phi = 0$ and $R_o F$ is the controlling parameter, c.f. eq. (15)). For $R_o F < \frac{1}{4}$ the values and variation of Φ indicate the presence of weak buoyancy waves, and the amplitude of Φ increases with R_o. As $R_o F$ traverses the band $[0.25, 0.5]$ the latter relationship is inverted and the Φ-amplitudes increase substantially. These changes reflect first the emergence and then the dominance of the non-linearly generated and non-balanced flow asymmetries.

4.4. *Synthesis of the results*

The simulations reported in the previous subsections record the nature of the flow patterns in the intermediate domain of $R_o F$ parameter space for three specific values of R_o. These simulations

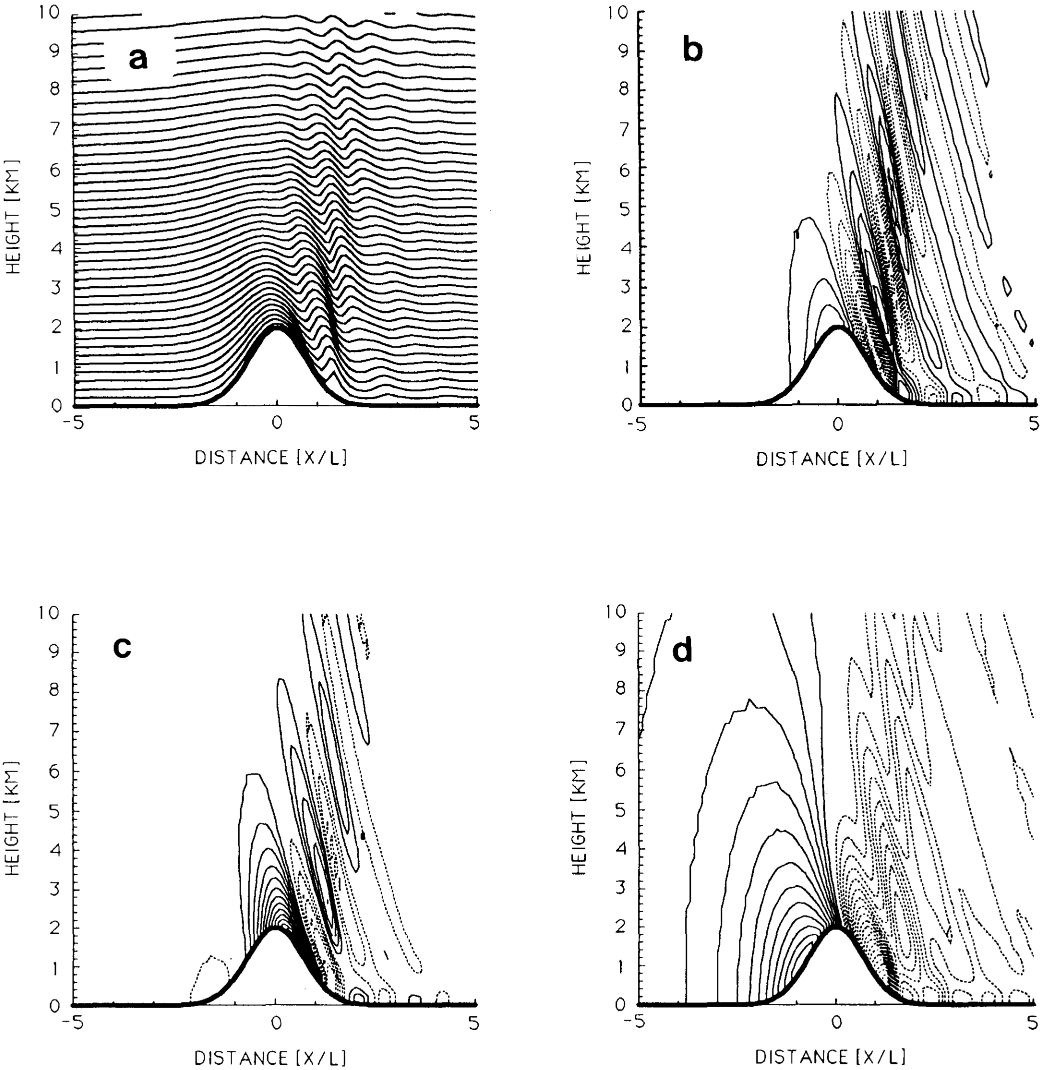

Fig. 13. Quasi-steady state orographic flow response for $R_o = 0.25$ and $F = 2$. (Display as for Fig. 3 but with no amplification.)

were presented for their representativity, and serve to illustrate the differing pathways to regime transition within the intermediate domain.

At one margin of the domain, viz. $R_o > 3$, the structures are akin to the much studied non-rotational case and the pathway to a regime transition with increasing F is via an increase to the critical value of the amplitude and steepness of the almost rotation-free buoyancy waves.

At the core of the intermediate domain, i.e., $R_o \sim 1$, an increase in F amplifies and distorts the low-level train of near-inertial waves such that the wave-crests tend to cusp and a train of buoyancy waves emerge from the crest and propagate along an inclined ray path away from the neighbourhood of the surface into the interior. The vertical propagation of energy away from the crest appears to counter the tendency for a cusp discontinuity

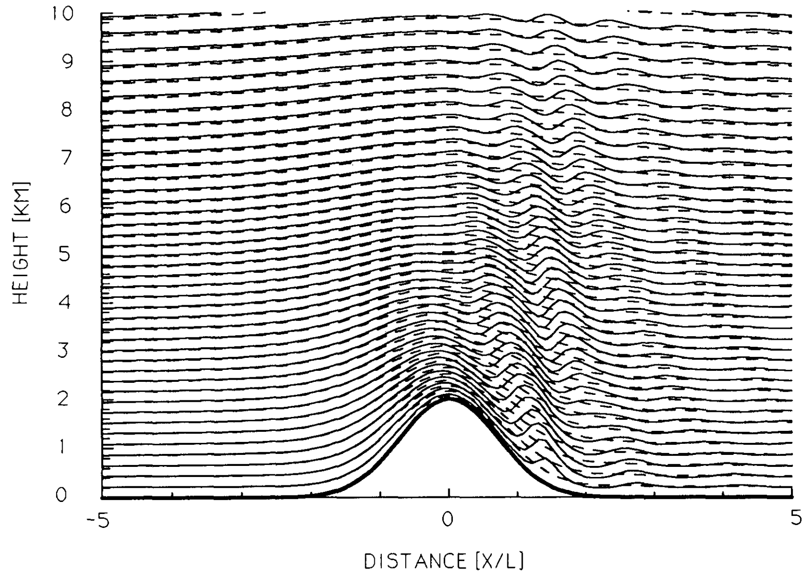

Fig. 14. The isentropic displacement fields for the quasi-balanced (dashed lines) and the full flow response (solid lines) illustrated for the two settings $(R_o, F) = (0.25, 2)$ and $(0.25, 0.01)$. There is a 200-fold amplification of the latter field.

and there is a concomitant reduction in the energy available for low-level horizontal transport to the next downstream wave crest.

At the rotationally-dominated margin of the intermediate domain, i.e., $R_o < \frac{1}{2}$, there is yet another pathway to regime transition. As F increases the balanced flow forces ageostrophic motion. The forcing occurs on a scale corresponding to a factor of ~ 4 contraction relative to that of the terrain and with little dependence upon $R_o F$ whilst the amplitude increases like $R_o^2(1 - R_o F)^{-3}$. One component of the resulting ageostrophic motion manifests itself as a ray path of buoyancy waves tracking away from the neighbourhood of the surface into the interior.

Thus there is appreciable buoyancy wave generation across the entire R_o band of the intermediate domain. As R_o decreases the source for the buoyancy waves changes continuously from direct orographic forcing to that linked with the cusping of a leeward train of low-level near-inertial waves and then to the forcing induced by the breakdown of balanced flow. It is this change that demarks the differing pathways to regime transition.

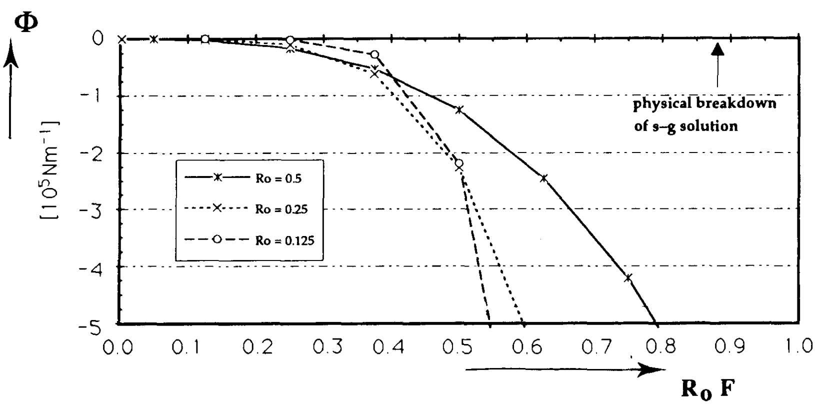

Fig. 15. Values of Φ, an indicator of buoyancy wave activity (see text for definition), displayed as a function of $R_o F$ for $R_o = (0.125, 0.25, 0.5)$.

5. Further remarks

Here we discuss some of the limitations of the approach adopted in this study. Thereafter we comment in turn upon the relationship of the present study to other idealised model studies, to observations, and to mesoscale numerical weather prediction.

Consideration of the adiabatic flow of an incident stream characterized by uniform velocity and statification over an infinite ridge, although a classical paradigm, is highly idealised. Theoretical and numerical model studies indicate that in the non-rotating limit significant modification of the flow response can be induced by diabatic effects (Jusem and Barcilon, 1985; Davies and Schär, 1986), planetary boundary layer (PBL) processes (Bougeault and Lacarrere, 1989; Richard et al., 1989) and non-uniform upstream conditions (Klemp and Lilly, 1975; Peltier and Clark, 1979; Durran, 1986, 1992). Moreover the dynamics of these flow modifications is often subtle, e.g., the incorporation of a PBL representation would modify the structure of the flow and/or the stratification of the incident airstream in the low layers, and thereby alter the "effective" value of F (in the case of pure mechanical turbulence) or conceivably establish a two-layer F-structure (in the case of a fair-weather PBL), and these changes could in turn yield starkly differing flow responses. For the f-plane setting of the present study, comparatively little is known of the influence of diabatic, PBL and a richer upstream flow structure, and our results are merely a forerunner for such studies.

From a numerical modelling standpoint, a critical issue is that both the finiteness of the horizontal grid and the use of a hydrostatic model precludes direct consideration of wave-overturning. In the present study attention was confined specifically to pre- and incipient flow tranition, and the occurrence of convective instability was excluded by taking advantage of the model's isentropic framework and adopting a positive definite algorithm for the prediction of the inverse of the static stability. This approach differs conceptually from the standard procedure used in hydrostatic models of introducing a convective adjustment parameterization scheme. In our model, incipient wave-overturning was accompanied by, and detected via, a marked increase in diffusive effects, and the adequacy of the approach for this purpose was verified in the non-rotating setting.

A key flow feature of the present study is the train of near-inertial low-level waves on the lee-side. This feature has been noted in previous idealised model studies. Pierrehumbert (1984) demonstrated the occurrence of a near-inertial linear wave train in the linear limit. Eliassen (1968) and Smith (1979) noted that the change in the doppler-shift of an inertia-buoyancy wave propagating vertically through a sheared flow could tranform it into an inertial wave and that thereafter it would propagate undamped horizontally, and Eliassen and Thorsteinsson (1984) provided examples of this latter effect. Also Lim (1975) derived nonlinear analytical solution for rotating shallow water flow over an infinite ridge, and showed that as the amplitude of the lee-side train of near-inertial waves increased they developed cusps and moreover at a critical value of the external parameters these steady-state, continuous solutions ceased to exist. In contrast the continuously stratified atmosphere allows vertical energy leakage away from the cusp region via propagation of buoyancy waves into the interior.

Another striking feature is the occurrence of buoyancy waves in flows over broad terrain ($R_o < 1$). Evidence of a buoyancy wave response in flow over such terrain is discernible in the nonlinear numerical simulations of Mason and Sykes (1978) and Pierrehumbert and Wyman (1985), and albeit only faintly in the laboratory experiments of Boyer and Biolley (1986). In the present study these waves were linked to the forcing of ageostrophic flow by the balanced flow field. This "geostrophic adjustment" is a comparatively simple prototype of the adjustment that can occur on the meso-scale as a result of scale contraction of balanced flow, e.g., during strong frontogenesis (Snyder et al., 1993).

Direct and definitive observations of the two forementioned phenomena will be difficult. Turbulence within the planetary boundary and unsteadiness of the incident airstream will both act to modify or curtail the appearance of near-inertial waves. Even if present, their pressure signal would be weak, and their horizontal scale and confinement to the lower levels would render detection of their wind fields problematic with the routine observational networks. The occurrence of cloud bands aligned parallel to a ridge at a distance comparable to the first lee-side crest, could form indirect evidence of their presence (c.f., Dirks et al., 1967). Likewise for buoyancy waves over broad terrain it would be difficult to distinguish between those attributable to scale-contraction and those associated with the smaller-scale height variance of the terrain.

In relation to modelling issues and mesoscale weather prediction we note that the explicit representation of near-inertial waves and the "scale contraction plus adjustment" process both require fine horizontal and vertical spatial resolution. Alternatively the implicit parameterization of their effects requires a representation of the momentum exchange associated with the indirectly induced buoyancy waves. In contrast to conventional gravity wave drag this exchange involves an additional internal transformation mechanism.

REFERENCES

Baines, P. G. 1987. Upstream blocking and airflow over mountains. *Ann. Rev. Fluid. Mech.* **19**, 75–97.

Bougeault, P. and Lacarrère, P. 1989. Parameterization of orography-induced turbulence in a meas-beta-scale model. *Mon. Wea. Rev.* **117**, 1872–1890.

Boyer, D. L. and Biolley, F. M. 1986. Linearly stratified, rotating flow over long ridges in a channel. *Phil. Trans. Roy. Soc. Lond.* **A318**, 411–438.

Davies, H. C. 1983. Limitations of some common lateral boundary schemes in regional NWP models. *Mon. Wea. Rev.* **111**, 1002–1012.

Davies, H. C. and Schär, Ch. 1986. Diabatic modification of airflow over mesoscale orographic ridge: a model study of the coupled response. *Quart. J. Roy. Met. Soc.* **112**, 711–730.

Davies, H. C. and Horn, J. 1988. Semi-geostrophic flow of a stratified atmosphere over elongated isentropic valleys and ridges. *Tellus* **40A**, 61–79.

Dirks, R. A., Mahlman, J. D. and Reiter, E. R. 1967. Evidence of a mesoscale wave phenomenon in the lee of the Rocky mountains. *Atmospheric Science Paper* **115**, Colorado State University, 29 pp.

Durran, D. R. 1986. Another look at down-slope winds. Part I: The development of analogs to supercritical flow in an infinitely deep, continuously stratified atmosphere. *J. Atmos. Sci.* **43**, 2527–2543.

Durran, D. R. 1986. Two-layer solutions to Long's equation for vertically propagating mountain waves: How good is linear theory? *Quart. J. Roy. Met. Soc.* **118**, 415–434.

Eliassen, A. 1968. On mesoscale mountain waves on the rotating earth. *Geofys. Publ.* **27**, 1–15.

Eliassen, A. and Palm, E. 1960. On the transfer of energy in stationary mountain waves. *Geofys. Publ.* **22**, 1–23.

Eliassen, A. and Raustein, E. 1970. A numerical integration experiment with a six-level atmospheric model with isentropic information surface. *Meteor. Ann.* **5**, 429–449.

Eliassen, A. and Kekustad, J. E. 1971. A numerical study of meso-scale mountain waves. *Geofys. Publ.* **28**, 1–13.

Eliassen, A. and Thorsteinsson, S. 1984. Numerical studies of stratified air flow over a mountain ridge on the rotating earth. *Tellus* **36A**, 172–186.

Gill, A. E. 1982. *Atmosphere-ocean dynamics*. Academic Press, New York, 662 pp.

Hsu, Y. G. and Arakawa, A. 1990. Numerical modelling of the atmosphere with an isentropic vertical coordinate. *Mon. Wea. Rev.* **118**, 1933–1959.

Jusem, H. C. and Barcilon, A. 1985. Simulation of moist, mountain waves with an anelastic model. *Geophys. Astrophys. Fluid Dynamics* **33**, 320–339.

Klemp, J. B. and Lilly, D. K. 1975. The dynamics of wave-induced downslope winds. *J. Atmos. Sci.* **32**, 320–339.

Klemp, J. B. and Lilly, D. K. 1978. Numerical simulation of hydrostatic mountain waves. *J. Atmos. Sci.* **35**, 78–107.

Krishnamurti, T. N. 1964. The finite amplitude mountain wave problem with entropy as vertical coordinate. *Mon. Wea. Rev.* **92**, 147–160.

Lilly, D. K. and Klemp, J. B. 1979. The effect of terrain shape on nonlinear hydrostatic mountain waves. *J. Fluid. Mech.* **95**, 241–261.

Lim, H. 1975. *Barotropic wave motions in rotating fluids*. PhD Thesis, University of Reading, pp. 250.

Long, R. R. 1953. Some aspects of the flow of stratified fluids (I). A theoretical investigation. *Tellus* **5**, 42–58.

Mason, P. J. and Sykes, R. I. 1978. On the interaction of topography and Ekman boundary layer pumping in a stratified atmosphere. *Quart. J. Roy. Met. Soc.* **104**, 475–490.

Mesinger, F. and Arakawa, A. 1976. *Numerical methods used in atmospheric models*. GARP-Publ. Series no. 17, vol. 1, 64 pp.

Miles, J. W. and Huppert, H. E. 1969. Lee waves in a stratified flow. Part IV. Perturbation approximation. *J. Fluid Mech.* **35**, 497–525.

Peltier, W. R. and Clark, T. L. 1979. The evolution and stability of finite-amplitude mountain waves. Part II: Surface wave drag and severe downslope winds. *J. Atmos. Sci.* **36**, 1498–1529.

Pierrehumbert, R. T. 1984. Linear results on the barrier effects of mesoscale mountains. *J. Atmos. Sci.* **41**, 1356–1367.

Pierrehumbert, R. T. 1985. Stratified semigeostrophic flow over two-dimensional topography in an unbounded atmosphere. *J. Atmos. Sci.* **41**, 1356–1367.

Pierrehumbert, R. T. and Wyman, B. 1985. Upstream effects of mesoscale mountains. *J. Atmos. Sci.* **42**, 977–1003.

Richard, E., Mascart, P. and Nickerson, E. C. 1989. The role of surface friction in downslope windstorms. *J. Appl. Met.* **28**, 241–251.

Sadourny, R. 1975. The dynamics of finite-difference models of the shallow-water equations. *J. Atmos. Sci.* **32**, 680–689.

Shapiro, M. A. 1974. The use of isentropic coordinates in the formation of objective analysis and numerical prediction models. *Atmosphere* **12**, 10–17.

Smith, R. B. 1977. The steepening of hydrostatic mountain waves. *J. Atmos. Sci.* **34**, 1634–1654.

Smith, R. B. 1979. The influence of the earth's rotation on mountain wave drag. *J. Atmos. Sci.* **36**, 177–180.

Smith, R. B. 1988. Linear theory of stratified flow past an isolated mountain in isosteric coordinates. *J. Atmos. Sci.* **45**, 3889–3896.

Smolarkiewicz, P. K. 1984. A fully multi-dimensional positive definite advection transport algorithm with small implicit diffusion. *J. Comp. Phys.* **54**, 325–362.

Snyder, C., Skamarock, W. C. and Rotunno, R. 1993. Frontal dynamics near and following frontal collapse. *J. Atmos. Sci.* **50**, 3194–3211.

Trüb, J. 1993. *Dynamical aspects of flow over Alpine-scale orography. A modeling perspective*. PhD thesis. ETH Zurich, Diss. No. 10339, 140 pp.